

Article

The Enhanced Moisture Absorption and Tensile Strength of PVA/*Uncaria gambir* Extract by Boric Acid as a Highly Moisture-Resistant, Anti-UV, and Strong Film for Food Packaging Applications

Dieter Rahmadiawan ¹, Hairul Abral ^{2,3,*}, Razan Muhammad Railis ², Ilham Chayri Iby ², Melbi Mahardika ^{3,4}, Dian Handayani ^{4,5}, Khiky Dwi Natrana ⁵, Dian Juliadmi ³ and Fazhar Akbar ³

¹ Department of Mechanical Engineering, Faculty of Engineering, Universitas Negeri Padang, Padang 25171, Indonesia

² Laboratory of Nanoscience and Technology, Department of Mechanical Engineering, Andalas University, Padang 25163, Indonesia

³ Research Center for Biomass and Bioproducts, National Research and Innovation Agency (BRIN), Cibinong Science Center, Cibinong 16911, Indonesia

⁴ Research Collaboration Center for Nanocellulose, BRIN-Andalas University, Padang 25163, Indonesia

⁵ Laboratory of Sumatran Biota, Faculty of Pharmacy, Andalas University, Padang 25163, Indonesia

* Correspondence: abral@eng.unand.ac.id



Citation: Rahmadiawan, D.; Abral, H.; Railis, R.M.; Iby, I.C.; Mahardika, M.; Handayani, D.; Natrana, K.D.; Juliadmi, D.; Akbar, F. The Enhanced Moisture Absorption and Tensile Strength of PVA/*Uncaria gambir* Extract by Boric Acid as a Highly Moisture-Resistant, Anti-UV, and Strong Film for Food Packaging Applications. *J. Compos. Sci.* **2022**, *6*, 337. <https://doi.org/10.3390/jcs6110337>

Academic Editor: Francesco Tornabene

Received: 4 October 2022

Accepted: 2 November 2022

Published: 4 November 2022

Publisher's Note: MDPI stays neutral with regard to jurisdictional claims in published maps and institutional affiliations.



Copyright: © 2022 by the authors. Licensee MDPI, Basel, Switzerland. This article is an open access article distributed under the terms and conditions of the Creative Commons Attribution (CC BY) license (<https://creativecommons.org/licenses/by/4.0/>).

Abstract: There is an increasing demand for food packaging materials that are safe for the environment and human health. Pure polyvinyl alcohol (PVA) film is non-toxic and transparent but has poor UV-light shielding, thermal and moisture resistance, and antibacterial activity. Our previous work prepared and characterized a biofilm derived from PVA and edible *Uncaria gambir* extract (UG). The film has antibacterial properties and is anti-UV and flexible. However, UG is hydrophilic, making this film have low moisture absorption. To improve these properties, we trialed adding boric acid (BA) and UG into the PVA. This present study aims to characterize pure PVA film and blend films resulting from mixing PVA (10%), BA (0.5%), and UG (1%). It was found that the PVA/UG/BA film presented the best performance in terms of UV light absorption, tensile properties, thermal and moisture resistance, and antibacterial activity. This blend sample absorbs about 98% of the UV light at 400 nm wavelength without significantly sacrificing transparency. These findings indicate that UG and BA could be advantageous in the preparation of moisture and thermal-resistant UV shielding films with low toxicity and high antibacterial properties based on PVA. They were also found to be strong enough for food packaging applications.

Keywords: phenolic compound; UV rays; moisture absorption; PVA-based film; tensile properties

1. Introduction

Nowadays, biomaterials play a crucial role in modern technology regarding sustainability [1]. It has been utilized in various applications, and one of many examples is biofilm [2,3]. In studying biofilm, discovering low-priced, non-toxic, biodegradable, and environmentally friendly food packaging materials is essential [4,5]. PVA has been used as a substitute for petroleum-based non-degradable materials to minimize the environmental impact of synthetic plastic waste [6]. This synthetic biopolymer material possesses high transparency, good biodegradability, low toxicity, and biocompatibility [7–11]. However, pure water-soluble sPVA film is transparent to UV light, has low tensile strength and low resistance to heat and moisture, and does not have antibacterial activity [12–14]. These drawbacks consequently limit the usefulness of PVA for food packaging. Many efforts have been carried out to minimize the weaknesses of PVA by mixing it with other materials. For example, disintegrated bacterial cellulose [15] and malleated chitin nanofibers [16,17]

improve fiSlms' mechanical and thermal properties. The introduction of ginger nanofibers has been proven to improve the antimicrobial activity, tensile strength, and heat resistance of PVA films [18].

High moisture resistance in food packaging materials is vital to retaining foodstuffs' taste, freshness, and shelf life [19]. However, due to its hydrophilic nature, PVA is sensitive to moisture [20]. Previous studies introduced boric acid into PVA to improve the moisture resistance of the blend film [20,21]. Boric acid can form strong hydrogen bonds with PVA molecules, reducing the hydroxyl groups' hydrophilicity [21,22]. However, it does not provide UV protection and antibacterial activities in the polymer film.

Some PVA-based films with high UV shielding and antimicrobial activity have been prepared using eco-friendly fillers, including sepia eumelanin [23], ZnO [24], and lignin [25,26]. Interestingly, Yingxiang Zhai et al. [27] introduced polyphenols in larch bark tannins as UV absorbers in PVA composite films to protect vitamin E from UV damage. Despite these developments, the challenge to obtain PVA films that are low-cost, eco-friendly, low-toxic, and transparent with good UV-shielding, water resistance, tensile, thermal properties, and antibacterial ability remains. We proposed a PVA with edible *Uncaria gambir* extract (UG) in our previous work. Specifically, this UG offers excellent UV light protection without sacrificing transparency [28]. It is inexpensive and non-toxic, and the tannin compound of UG provides strong antibacterial activity [29].

Moreover, it prevents metal from corrosion, which is also suitable for various applications [30]. However, UG is hydrophilic and has a low moisture absorption level in the film. We proposed a novel strategy to overcome this deficiency by introducing boric acid into PVA and UG to prepare anti-UV, antibacterial, strong, high thermal resistant, and high moisture resistant films. These characterizations of the blended film have not been explored until now. Therefore, this present work characterizes PVA-based films blended with UG, BA, and UG/BA. The morphology of pure PVA film and PVA-based blends was observed using field emission scanning electron microscopy (FESEM). Transparency, moisture absorption, tensile properties, thermal resistance, and antibacterial activity were measured, and X-ray diffraction (XRD) and Fourier-transform infrared spectroscopy (FTIR) were performed on the films.

2. Materials and Methods

2.1. Materials

Uncaria gambir extract powder containing about 90% catechins was purchased from the Sumatran Biota Laboratory, Universitas Andalas. Distilled water was supplied by a Local Chemical Store in Padang, Indonesia. Polyvinyl alcohol (Mw 89,000–98,000 g/mol, 99% hydrolyzed) was obtained from Sigma-Aldrich Pte. Ltd., Singapore. Reagent-grade boric acid (H₃BO₃) with >99.5% purity was acquired from Puduk Scientific (Jakarta, Indonesia).

2.2. Sample Preparation

UG gambir suspension purification: 1% UG was incorporated into distilled water (100 mL). The suspension was stirred by a magnetic stirrer (MS-H280-Pro, Scilogex, Berlin, CT, USA) at 500 rpm for 30 min for homogenization. The solution was centrifuged by a centrifuge apparatus at 2000 rpm for 30 min to separate immiscible liquids or sediment-suspended solids.

PVA film: Distilled water (100 mL) and PVA (10 g) were mixed. Using the magnetic stirrer (MS-H280-Pro, Scilogex, USA), the mixture was heated at 70 °C and 500 rpm for 2 h until gelatinized. An ultrasonic homogenizer sonicated the resulting gel at 600 W for 5 min. The treated gel cast in a Petri dish was dried for 20 h in a 50 °C vacuum drying oven at 0.6 MPa.

PVA/BA blend film: BA (0.5 wt% total solutions of PVA and distilled water) and PVA (10 g) were incorporated into distilled water (100 mL). The blend was heated with the magnetic stirrer at 70 °C and 500 rpm for 2 h until gelatinization.

The resulting gel was treated for 5 min using 600 W in an ultrasonic homogenizer. The sonicated gel was cast in a Petri dish and dried for 20 h in a 50 °C vacuum-drying oven at 0.6 MPa.

PVA/UG blend film: The suspension of pure UG (1 wt%), PVA (10 g), and distilled water (100 mL) was heated with the magnetic stirrer at 70 °C and 500 rpm for 2 h until gelatinization. The resulting gel was treated with a 600 W ultrasonic homogenizer for 5 min. The sonicated gel was cast in a Petri dish and dried for 20 h in a 50 °C vacuum drying oven at 0.6 MPa.

PVA/UG/BA blend film: The suspension (10 g PVA, 1 wt% UG, 0.5 wt% BA, and 100 mL distilled water) was heated by the magnetic stirrer at 70 °C and 500 rpm for 2 h until gelatinization. The resulting gel was sonicated at 600 W for 5 min. The sonicated gel was cast in a Petri dish and dried for 20 h in a 50 °C vacuum drying oven at 0.6 MPa.

2.3. FESEM Morphology

A field emission scanning electron microscope (FESEM Quattro S, Thermo Fisher Scientific, Waltham, MA, USA) was used to observe the morphological fracture surfaces of the films. The sample was placed on the carbon tube. The FESEM image of the film was recorded with different (250, 500, and 2000) magnifications under a high vacuum at 3.0 kV accelerating voltage.

2.4. Film Transparency

The standard method ASTM D638-type V was used for tensile testing (ASTM D638-V 2012). The tensile strength (TS), tensile modulus (TM), and elongation at break (EB) of the sample were measured using a Com-Ten testing machine 95T. All samples before testing were stored in a closed desiccator (50% RH, 25 °C) for 48 h. The tensile tests were repeated five times for each film. A Shimadzu UV 1800 spectrophotometer was used to measure the transparency of films according to ASTM D 1003-00 [31]. An equal-weight rectangular sample (10 mm × 25 mm) was placed in the spectrophotometer by a transmittance spectrum of 200 to 800 nm. The transparency of the film is based on the area under the transmittance curve.

2.5. Tensile Properties

The tensile test used the ASTM D638-type V standard [32]. The width and thickness of the sample were measured via an optical microscope (Olympus Stereo Microscope SZX10, Evident, Japan) to get the sample dimensions accurately. The tensile curve, including tensile strength, elastic modulus, and elongation break of the film, was obtained using the Universal Testing Machine (UTM) (AGS-X series 5 kN, Shimadzu, Japan). A 30 mm/min tensile test speed was used. Tensile tests were repeated five times for each sample.

2.6. FTIR

FTIR spectra were performed using an Attenuated Total Reflectance-Fourier Transform Infra-Red (ATR)-FTIR spectroscopic instrument equipped with a UATR unit cell from PerkinElmer (Spectrum two) (PerkinElmer Corporation, Waltham, MA, USA). The sample was placed on the diamond crystal. Next, the dried film was scanned from 4000–400 cm⁻¹ at a resolution of 4 cm⁻¹ with 32 scans. The spectrum at a wavelength was taken by pressing the torque knob with the same pressure.

2.7. X-ray Diffraction

A thermal resistance instrument (DTG-60, Shimadzu, Japan) was used to measure the sample's TGA and DTG. A nitrogen flow rate of 50 mL/min and a heating rate of 10 °C/min were performed while testing the sample. X-ray diffraction pattern of samples was obtained using an instrument from Shimadzu XRD-700 Maxima X series (Shimadzu Corp., Kyoto, Japan). The testing was carried out at 24 °C, 40 kV, and 30 mA using Cu K α radiation ($\lambda = 0.15406$ nm). The sample was scanned from $2\theta = 10^\circ$ to 50° every 2° per

min. A Gaussian function was used to calculate the area of the crystalline and amorphous regions. The crystallinity index (CI) of the sample was calculated by Equation (1) [33]:

$$CI (\%) = (A_c / A_a + A_c) \times 100\% \quad (1)$$

where A_c is the integrated area for the crystalline region under the curve at $2\theta = 20^\circ$ – 23° . A_a is the area of the amorphous section at $2\theta = 15^\circ$ – 16° .

2.8. Thermogravimetry Analysis (TGA) and Derivative (DTG)

A thermal analysis instrument (TGA 4000, PerkinElmer, Hopkinton, MA, USA) was used to measure the TGA and DTG of samples. The sample (about 10 mg) was positioned on a microbalance inside the furnace. A nitrogen flow rate and the heating rate were set up at 20 mL/min and 10 °C/min, respectively. The test was carried out from 30 °C up to 600 °C. Pyris software (Version 11, Pyris, Washington, MA, USA) was used to examine weight loss, weight loss rate, and residue percentages.

2.9. Moisture Absorption

The measurement of moisture absorption (MA) was carried out using a previously described method [19]. All film samples were dried until a constant weight was reached in a drying oven (Memmert Germany, Model 55 UN) at 50 °C. The dried films were stored in a closed chamber (75% RH at 25 °C). The samples were weighed by a precision balance (Kenko, a 0.1 mg accuracy) every 30 min for 7 h. MA was determined using Equation (2):

$$MA = (w_h - w_o) / w_o \quad (2)$$

where w_h and w_o are the sample's final weight and initial weight. MA testing was repeated five times per film.

2.10. Antimicrobial Activity

As carried out in a previous study, the antimicrobial resistance of pure PVA and blend films was determined using the agar diffusion method [34]. The human pathogenic bacteria and fungi used were *Staphylococcus aureus* (SA), *Escherichia coli* (EC), *Pseudomonas aeruginosa* (PA), and the fungus *Candida albicans* (CA). An inoculant of a 100 µL suspension of bacteria or fungi was spread evenly on the surface of Nutrient Agar (NA) media for bacterial culture or Sabouraud Dextrose Agar (SDA) media for fungal cultures.

Subsequently, a disk of each film (6 mm diameter) was placed on top of the inoculated media, and the inoculant was allowed to grow for 24 h at 30 °C. Chloramphenicol and nystatin were positive controls for bacteria and fungi, respectively. The experiment was repeated three times for each film. The clear area formed around the film disk was not overgrown with the test microbe. This was measured and recorded.

2.11. Statistical Analysis

The tensile property and moisture resistance data were analyzed using an ANOVA. Duncan's multiple range test was applied for further analysis. Differences between samples were found to be significant at $p \leq 0.05$.

3. Results and Discussions

3.1. UV and Visible Light Transparency

Figure 1 shows the appearance of the film surface for each sample. Films without UG (Figure 1a,b) are highly transparent. After introducing the UG, the transparency of the movie became lower (Figure 1c,d). The UG-mixed blend films were still clear enough to be seen easily. An Andalus University emblem is clearly observable under the PVA/UG/BA film, as shown in Figure 1e.

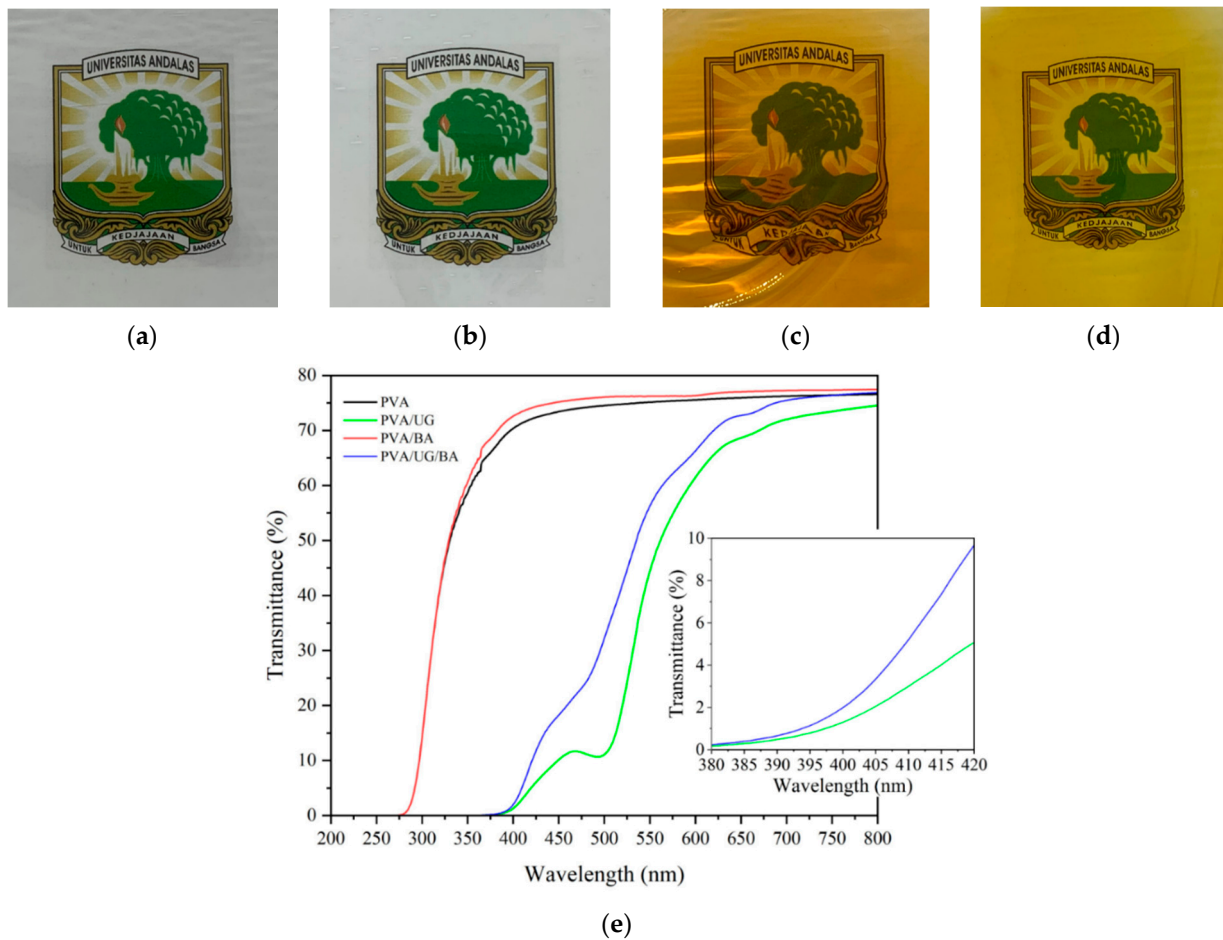


Figure 1. Photographs of the film for pure PVA (a); PVA/BA (b); PVA/UG (c); PVA/UG/BA (d). The light transmittance curves (e).

The UV spectrum can be categorized into three regions, i.e., UV-C (220–280 nm), UV-B (280–320 nm), and UV-A (320–400 nm) [23]. Figure 1e shows the transparency curve from the 200–800 nm wavelength range. Pure PVA/BA is the most transparent film in this wavelength range due to the lowest light scattering. Samples without UG transmitted UV light (below 400 nm wavelength). For example, the transmittance values of the PVA film and PVA/BA blend at 400 nm wavelength were 70.4% and 72.6%, respectively (Table 1). After adding UG into the PVA film, the blend film absorbs UV light effectively. The PVA/UG shows the best UV absorption performance. This film protected about 99% of UV rays at 400 nm. In detail, UV-C and UV-B light were 100% blocked and UV-A 99%. The high UV light absorption is attributable to the high catechin content of the UG [35,36]. This phenolic compounds and other chromophores in the catechin are responsible for absorbing UV rays and dissipating the absorbed energy [25,37]. This result agrees with previous work that demonstrated high UV light absorption of a composite film mixed with tannins containing polyphenols [27]. Remarkably, after adding BA to the PVA/UG suspension, the visible light transparency performance of the PVA/UG/BA film increased without a significant decrease in UV light absorption capacity. The transmitted light of this film at 650 nm was 72.7%, 6% higher than PVA/UG (68.7%), corresponding to a lower light scattering in the PVA/UG/BA film.

3.2. Cross-Section FESEM Images

Figure 2 shows the FESEM fractured surface in a cross-section of tensile samples for pure PVA (a,b), PVA/BA (c), PVA/UG (d), and PVA/UG/BA (e). Pure PVA shows a pulled-out segment (orange arrow film in Figure 2a) and smooth surfaces (orange dash line

box). This sample also presents fibrous surface fracture (white arrow in Figure 2b). These surface appearances correspond to high plastic deformation due to low crosslinking density between polymer chains. After introducing the UG and BA to PVA, no fibrous or pulled-out segments were visible in blend films. This finding was due to reduced PVA chain mobility from increased interlinking bonds. The fracture surface of PVA/BA is shinier and rougher (Figure 2c) than pure PVA (Figure 2a). This shiny appearance is due to more reflected light by the surface of the rigid sample. The coarser texture was due to the longer tortuous crack tip growth passing through the weakest part of the chain structure [28]. The rough display corresponds to the inhibition of crack growth resulting from the strong crosslinking interactions between PVA, UG, and BA molecules. The crosslink density increased with the higher blend concentration in PVA, thus increasing surface roughness (Figure 2d,e). Microscopic beach marks (red arrow in Figure 2e) are due to tortuous cracks resulting from the disruption of crack progress [38]. This is because of the low tensile strength of the PVA/UG/BA sample, which is consistent with tensile test properties. The strong crosslinker interaction from UG and BA binds the free hydroxyl group of the polymer, causing the molecules to be harder to move.

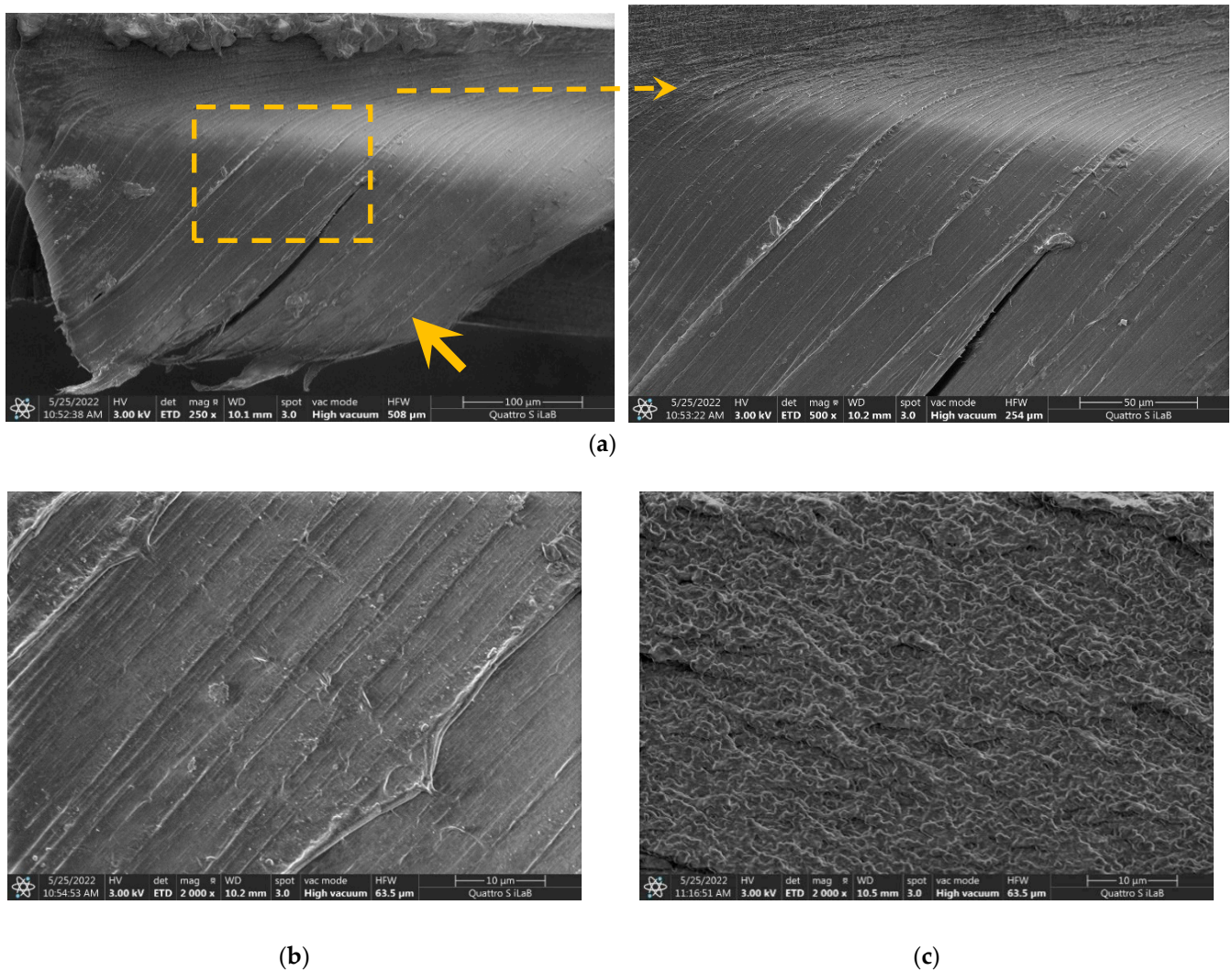


Figure 2. Cont.

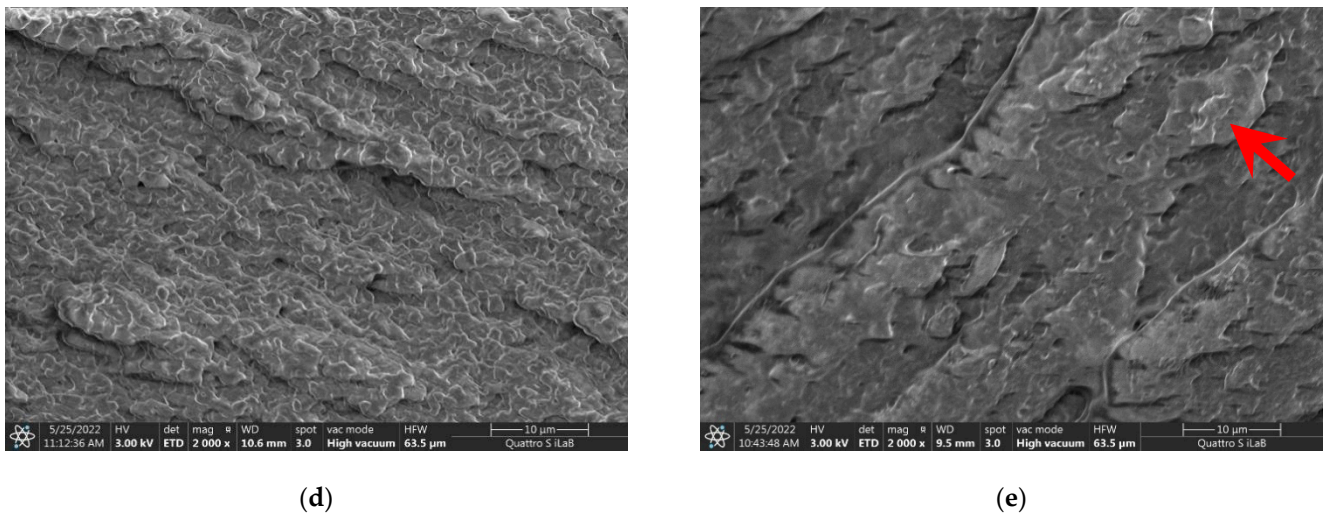


Figure 2. FESEM fracture surface of the PVA film (a,b) and the blend films PVA/BA (c), PVA/UG (d), and PVA/UG/BA (e). Tortuous cracks resulting from the disruption of crack progress (red arrow).

3.3. FTIR Spectrum

Figure 3 displays FTIR curves of samples prepared with different treatments. The prominent peaks at about 3271 , 2915 , and 1655 cm^{-1} correspond to O–H stretching, C–H stretching, and O–H of absorbed water, respectively [39]. All the samples show similar patterns confirming the treatments did not alter the nature of the functional groups of the PVA. However, introducing BA or/and UG to PVA changed the wavenumber and the peak intensity in the FTIR curves. For example, the addition of UG to PVA shifted the wavenumber of O–H stretching of the blends from 3271 cm^{-1} (PVA) to 3264 cm^{-1} (the PVA/UG). The shifting is attributable to increasing hydrogen bond density resulting from more contact of the free –OH groups present in PVA, BA, and UG assisted by high temperature during sample preparation. This higher crosslinking ratio reduced the number of free hydroxyl groups, thus weakening the peak intensity of hydroxyl functional groups.

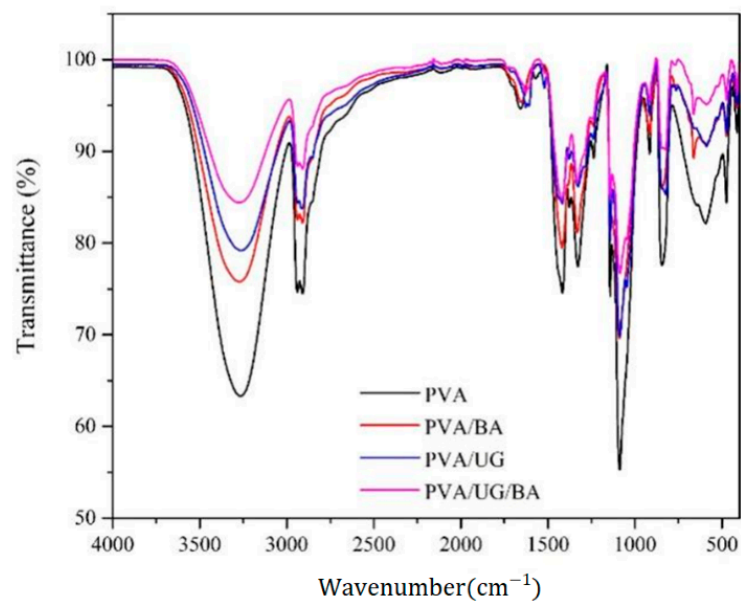


Figure 3. FTIR of PVA and the blend films.

The PVA film shows the lowest T-value of O–H stretching vibration (63%) due to the largest free hydroxyl fraction. After adding BA and UG into the PVA suspension, the O–H stretching intensity in the films shifted. The T-value for O–H groups for the PVA/BA film

is 76%, and the PVA/UG is 79%. The weakest peak intensity of these O–H groups was measured on the PVA/UG/BA film ($T = 84\%$), confirming the lowest number of free O–H groups. The reduced number of free O–H groups corresponds to the increased crosslinking ratio and hydrogen bonds of the blends with PVA molecules [40].

3.4. X-ray Diffraction

Figure 4 displays the X-ray diffraction curve of the PVA-based films with and without UG and BA loading. A major diffraction peak at $2\theta = 20^\circ$, attributed to (101) crystal plane diffraction, characterizes PVA [26]. Table 1 shows the value of each sample in light transmittance (at 400 nm) from Figure 1b, CI from Figure 4, d -lattice plane spacing from XRD, and T_{\max} from Figure 5b. The highest peak shifting was measured on the PVA/UG/BA, probably resulting from the largest shift in the d -spacing [Å] of (101) planes [29]. The area under the XRD curve in the range of $10\text{--}30^\circ$ corresponds to the degree of crystallinity index (CI). The clearer the area, the lower the CI value [41]. The CI of pure PVA film was 27.7%, higher than PVA/BA (25.9%) and PVA/UG (24.5%). The decrease in CI resulted from BA and/or UG acting as a crosslinker for PVA chains in the amorphous region, consequently inhibiting the crystalline alignment of polymer chains [41]. Hence, adding UG and BA to PVA resulted in the lowest CI value (23.9%) of PVA/UG/BA film. This result is in agreement with previous work [41].

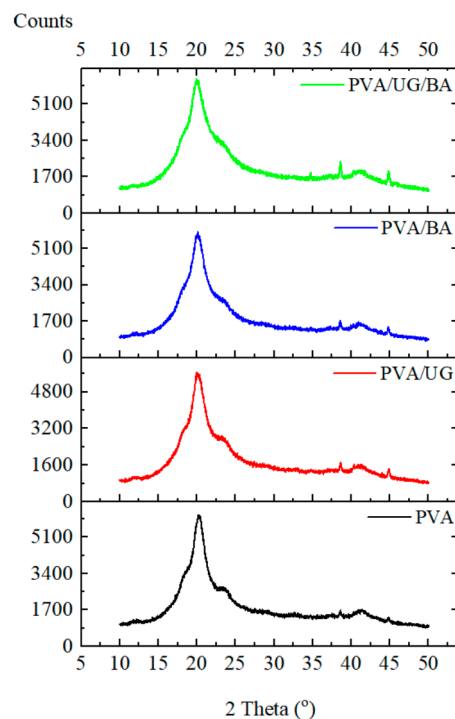


Figure 4. XRD pattern of PVA and the blend films.

Table 1. Light transmittance from Figure 1b, CI from Figure 4, d -lattice plane spacing from X-ray diffraction data, and T_{\max} from Figure 5b.

Film Samples	Transmittance (%) at 400 nm	2 Theta (Degree)	Crystallinity (%) of (101) Plane	d -Spacing [Å] of (101) Plane	T_{\max} (°C) at Second Weight Loss
PVA	70.4	20.17	27.7	4.398	312
PVA/BA	72.6	20.05	25.9	4.425	355
PVA/UG	1.3	20.14	24.5	4.406	358
PVA/UG/BA	2.0	20.06	23.9	4.423	368

3.5. Thermal Resistance

The thermal stabilities of films were characterized using TGA and DTG. Figure 5 presents the thermal characteristic of pure PVA and the blend films. Each TGA curve (Figure 5a) shows a three-step thermal degradation with temperature increases. At first, the slight weight loss from 60 °C to 150 °C corresponds to the evaporation of absorbed water [15,42]. In the second stage, the rapid drop of sample weight (270–450 °C) was due to the PVA, BA, and UG decomposition [26]. Figure 5b and Table 1 display values for temperatures of the maximum decomposition rate (T_{max}) of films during the second weight-loss period. After mixing the UG or/and the BA with the PVA, the T_{max} increased. The T_{max} value of the PVA/BA and PVA/UG films were 361.24 °C and 369.49 °C, respectively, around 14% and 15% higher than that of pure PVA (324.28 °C). This result is probably due to the increasing crosslinking polymer chain ratio, resulting in higher activation energy needed to decompose the blend films [43,44]. Hydroxyl groups of PVA, BA, and UG interact strongly via interfacial hydrogen bonding [45]. This phenomenon is consistent with the PVA/UG/BA film showing the highest thermal resistance ($T_{max} = 369.49$ °C). For further heating over 470 °C, a third weight loss displays a final decomposition to ash [7].

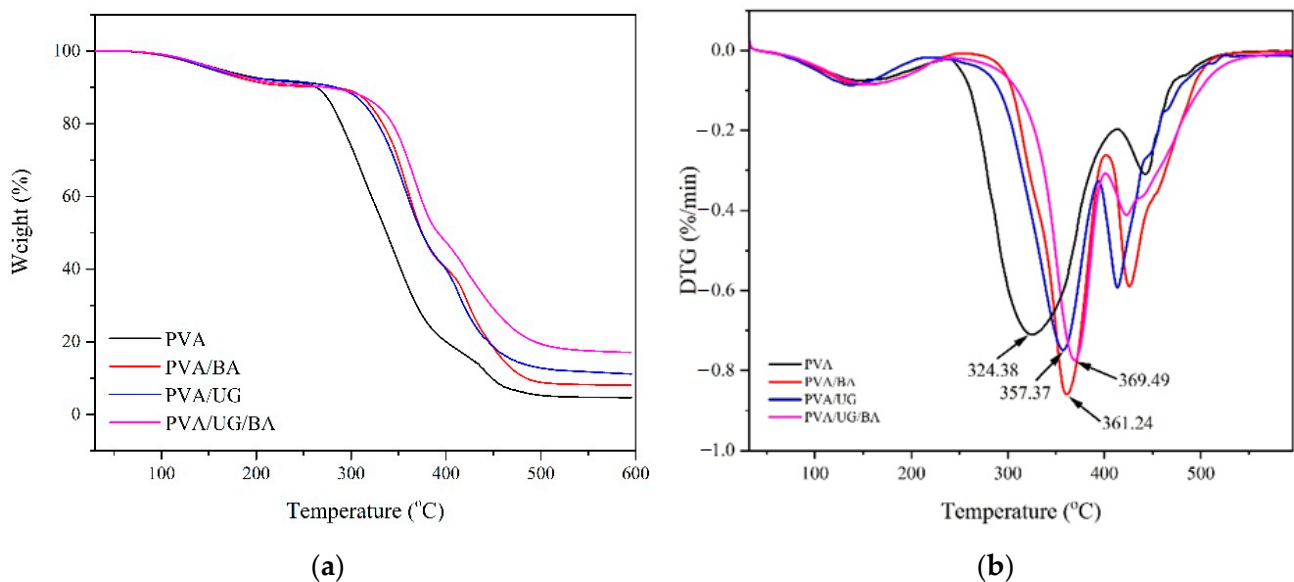


Figure 5. Thermal properties (TGA (a) and DTG (b) for PVA and blends.

3.6. Tensile Properties

Figure 6 presents the tensile properties of samples. The stress-strain characteristic curve of pure PVA and the blend films (Figure 6a) show that all films experienced elastic and plastic deformation. PVA had low performance in tensile strength (TS), modulus of elasticity (ME), and high elongation at break (EB) and area under the curve (sample toughness (TN)). After blending the PVA with UG and BA, the characteristic curve of the blends changed. TS and ME increased, and EB and TN decreased. Besides, a knee-shaped change in slope between elastic and plastic deformation, a red arrow in Figure 6a, became sharper as fillers were added to the PVA. After introducing UG or/and BA to PVA, the position of this change in slope in the curve also increased, corresponding to increasing yield strength. The increased sharpness of the knee-shaped change in slope and higher yield strength value could be due to a reduction in the slippage between the extended PVA chains. The highest yield point was present in the PVA/UG/BA due to the most interconnected PVA polymer fraction. This result is consistent with the XRD pattern (Figure 4), displaying the decreasing CI value as the crosslinks in the PVA increased. With subsequent elongation, this strength dropped dramatically, probably due to more breaking fractions of interconnected chains in the amorphous region [46]. With even further

extension, the film strength increased, corresponding to strain-hardening that results from breaking and extending polymer chains in the crystal fraction. As shown in Figure 6b, PVA had low average values of TS (43.9 MPa) and ME (0.25 GPa) but remarkably high EB (212.3%) and TN (43.1 MJ/m³). This high toughness is attributable to the high degree of polymer chain fraction unconnected via intermolecular hydrogen bonds. Thus, the energy required for PVA chain slippage resulting in extension was lower than what is required for crack propagation. This finding is consistent with the fibrous and pulled-out PVA section in Figure 2a,b.

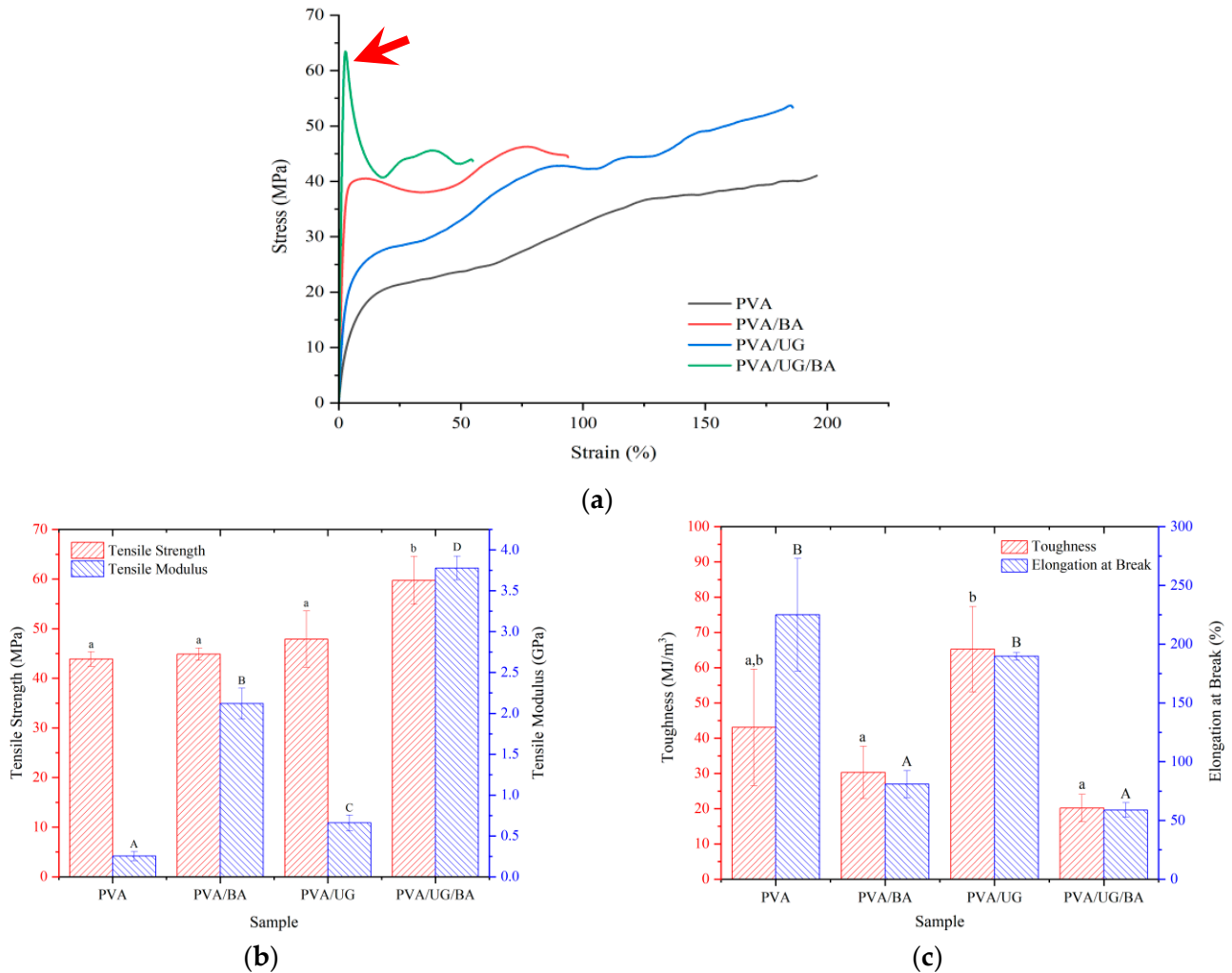


Figure 6. Stress–strain curve of samples (a), the average value of TS and TM (b), and TN and EB (c) for samples. A significant difference in mean values ($p \leq 0.05$) is indicated with different letters (a, b, A, B, C, D).

After adding BA, UG, or UG/BA to PVA, TS increased from 43.9 to 44.9, 47.9, and 57.7 MPa, respectively. These higher TS values are attributable to an increase in interlinking bonds, thus, reducing the PVA chain mobility. This result agrees with the fracture surface of these blends having no visible fibrous and pulled-out polymer section (Figure 2c–e). Although the TS of PVA/UG is higher than that of PVA/BA, the elongation at break of the PVA/UG film (170.5%) was twice as high as that of the PVA/BA film (75.8%), as shown in Figure 6c. Besides, the ME of PVA/BA was 2.1 GPa, higher than that of PVA/UG (0.7 GPa). This finding confirmed that PVA mixed with 0.5% BA became more brittle than when mixed with 1% UG.

Furthermore, combining crosslinkers (UG and BA) to PVA resulted in the highest ME of 3.7 GPa, but the lowest EB of 48.2% and TN of 20.2 MJ/m³. This result shows that

the PVA/UG/BA had the most rigid chain structure resisting slippage because it had the highest intermolecular crosslinking. This phenomenon is consistent with the FTIR curve (Figure 3), displaying the weaker intensity of peak transmittance and a shift of -OH bands with increased filler loading.

3.7. Moisture Absorption

Figure 7 displays the moisture absorption (MA) for the PVA film and blend films. Introducing the blends to PVA decreased the average MA value. The MA of PVA in an RH 75% humid chamber for 480 min was about 5.0%. The PVA/UG/BA blend film had the highest moisture resistance, with only 0.7% absorbed after eight hours. This improvement in MA resistance of this blend film was significant ($p \leq 0.05$) due to the addition of the crosslinking (BA and UG), forming hydrogen bonding between PVA chains, thus decreasing the number of free hydroxyl groups [18]. As a result, the ability of water molecules to diffuse into the blend film via Fickian diffusion decreased. This result is consistent with the FTIR curve for PVA/UG/BA film (Figure 4), showing the weakest peak intensity of the hydroxyl functional groups.

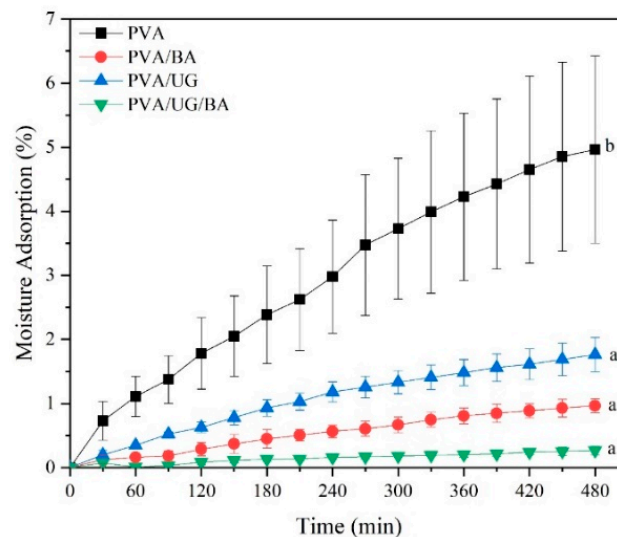


Figure 7. Average moisture absorption value of films. A significant difference in mean values ($p \leq 0.05$) is indicated with different letters (a, b).

3.8. Antimicrobial Properties

The antibacterial characteristics of samples are shown in Figure 8. The antimicrobial resistance of the film against pathogenic microbes is shown in Table 2, where the diameter of the inhibition zone (mm) reflects the sensitivity of the microorganisms used in the films. The antibacterial activity of the mixed film was higher than that of pure PVA. These films inhibited the growth of the test bacteria with an inhibition zone ranging from 6.0 ± 0.3 to 10.6 ± 0.1 mm. Similar to the results of previous studies, the mixed UG film could not inhibit the growth of the yeast *Candida albicans* due to the relatively small concentration of UG [28,47]. The presence of antibacterial polyphenol compounds (catechins) is the source of the antibacterial activity in mixed films [48,49]. The active components in catechin can destroy the plasma cell membrane resulting in the loss of intracellular components, thus the death of bacteria [44].

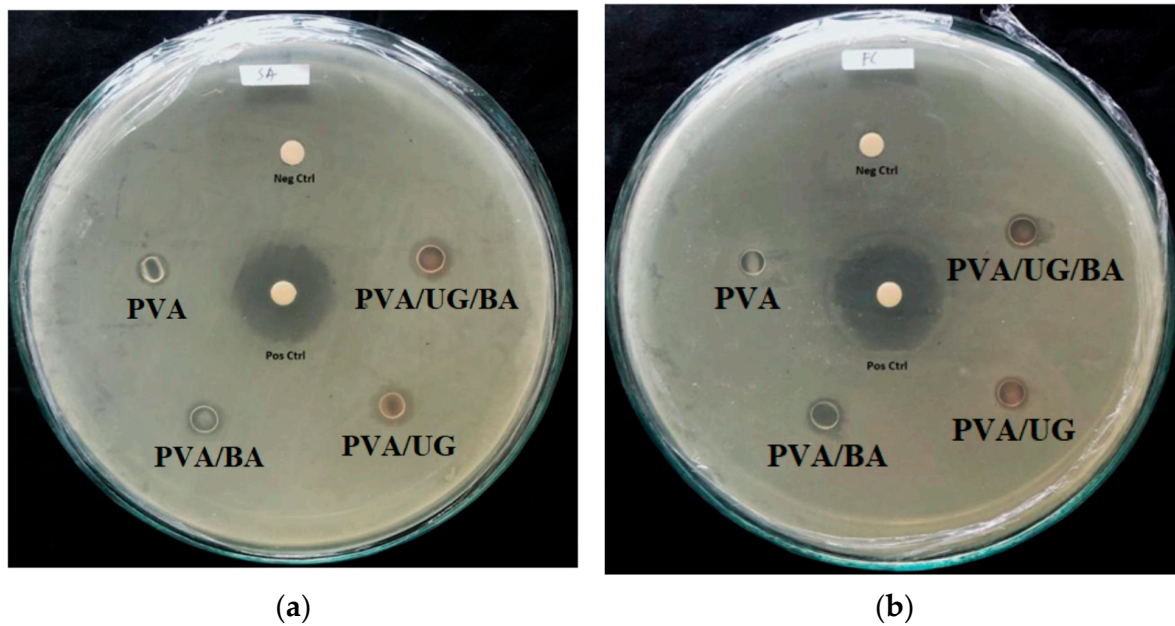


Figure 8. Antibacterial characteristics of samples (red arrow on transparent area diameter) against (a) *Staphylococcus aureus* (SA) and (b) *Escherichia coli* (EC). (Neg Ctrl) = negative control; (Pos Ctrl) = positive control (chloramphenicol).

Table 2. Antimicrobial resistance of samples.

Samples	Diameter of Inhibition Zone Antimicrobial Activity (mm)			
	SA &	PA &	EC &	CA &
PVA	6.0 ± 0.3	7.0 ± 0.7	6.5 ± 0.2	-
PVA/BA	9.2 ± 0.3	9.4 ± 0.6	10.2 ± 1.3	-
PVA/UG	10.5 ± 0.1	9.5 ± 0.2	9.9 ± 0.9	-
PVA/UG/BA	10.6 ± 0.1	10.5 ± 0.5	9.1 ± 0.3	-
Positive control	22.4	23.1	23.5	25.2

& *Staphylococcus aureus* (SA), *Pseudomonas aeruginosa* (PA), *Escherichia coli* (EC), and *Candida albicans* (CA).

4. Conclusions

Some properties of PVA-based film were enhanced when blended with boric acid and/or edible and inexpensive *Uncaria gambir*. Introducing the BA and the UG in the PVA matrix improved UV light protection, moisture resistance, antibacterial activity, and tensile and thermal properties. In this present study, the PVA/UG/BA blend film shows the best performance in the case of the above properties. This film inhibited 98% of UV light and had a TS of 57.7 MPa (31.81% higher than pure PVA film), a TN of 20.2 MJ/m³ (53.82% lower than PVA), and T_{max} of 369.49 °C (14% higher than pure PVA). This blend film had antibacterial resistance but no antifungal activity against *Candida albicans* (CA). These results suggest that the PVA/UG/BA blend film could be used as an alternative, environmentally friendly, low-cost, and non-toxic substance for food packaging applications.

Author Contributions: Data curation, I.C.I., M.M., D.H., D.J. and F.A.; Formal analysis, H.A., D.H. and D.J.; Funding acquisition, H.A.; Investigation, H.A., R.M.R. and K.D.N.; Resources, I.C.I.; Software, R.M.R. and K.D.N.; Supervision, D.R.; Visualization, M.M.; Writing—original draft, H.A.; Writing—review & editing, D.R. and D.H. All authors have read and agreed to the published version of the manuscript.

Funding: This research received no external funding.

Institutional Review Board Statement: Not applicable.

Informed Consent Statement: Not applicable.

Data Availability Statement: The raw/processed data required to reproduce these findings cannot be shared at this time due to technical or time limitations. Raw data will be provided on request.

Acknowledgments: The authors gratefully acknowledge the Directorate General of Higher Education for supporting research funding with project Penelitian Dasar Kompetitif Nasional 2022 (T/45/UN.16.17/PT.01.03/PDKN-Material Maju/2022).

Conflicts of Interest: The authors declare that they have no known competing financial interests or personal relationships that could have appeared to influence the work reported in this paper.

References

1. Rahmadiawan, D.; Asfhattahi, N.; Nasruddin, N.; Saidur, R.; Arifuzzaman, A.; Mohammed, H.A. MXene Based Palm Oil Methyl Ester as an Effective Heat Transfer Fluid. *J. Nano Res.* **2021**, *68*, 17–34. [[CrossRef](#)]
2. Cao, X.; Huang, J.; He, Y.; Hu, C.; Zhang, Q.; Yin, X.; Wu, W.; Li, R.K.Y. Biodegradable and renewable UV-shielding polylactide composites containing hierarchical structured POSS functionalized lignin. *Int. J. Biol. Macromol.* **2021**, *188*, 323–332. [[CrossRef](#)] [[PubMed](#)]
3. Wu, W.; Liu, T.; Deng, X.; Sun, Q.; Cao, X.; Feng, Y.; Wang, B.; Roy, V.A.L.; Li, R.K.Y. Ecofriendly UV-protective films based on poly(propylene carbonate) biocomposites filled with TiO₂ decorated lignin. *Int. J. Biol. Macromol.* **2019**, *126*, 1030–1036. [[CrossRef](#)] [[PubMed](#)]
4. Rahmadiawan, D.; Abrial, H.; Yesa, W.H.; Handayani, D.; Sandrawati, N.; Sugiarti, E.; Muslimin, A.N.; Sapuan, S.M.; Ilyas, R.A. White Ginger Nanocellulose as Effective Reinforcement and Antimicrobial Polyvinyl Alcohol/ZnO Hybrid Biocomposite Films Additive for Food Packaging Applications. *J. Compos. Sci.* **2022**, *6*, 316. [[CrossRef](#)]
5. Atta, O.M.; Manan, S.; Shahzad, A.; Ul-Islam, M.; Ullah, M.W.; Yang, G. Biobased materials for active food packaging: A review. *Food Hydrocoll.* **2022**, *125*, 107419. [[CrossRef](#)]
6. Haghighi, H.; Gullo, M.; La China, S.; Pfeifer, F.; Siesler, H.W.; Licciardello, F.; Pulvirenti, A. Characterization of bio-nanocomposite films based on gelatin/polyvinyl alcohol blend reinforced with bacterial cellulose nanowhiskers for food packaging applications. *Food Hydrocoll.* **2021**, *113*, 106454. [[CrossRef](#)]
7. Abrial, H.; Atmajaya, A.; Mahardika, M.; Hafizulhaq, F.; Kadriadi; Handayani, D.; Sapuan, S.M.; Ilyas, R.A. Effect of ultrasonication duration of polyvinyl alcohol (PVA) gel on characterizations of PVA film. *J. Mater. Res. Technol.* **2020**, *9*, 2477–2486. [[CrossRef](#)]
8. Heiba, Z.K.; Bakr Mohamed, M.; Ahmed, S.I. Exploring the physical properties of PVA/PEG polymeric material upon doping with nano gadolinium oxide: Exploring the physical properties of PVA/PEG polymeric material. *Alex. Eng. J.* **2022**, *61*, 3375–3383. [[CrossRef](#)]
9. Gadhve, R.V.; Vineeth, S.K.; Mahanwar, P.A.; Gadekar, P.T. Effect of addition of boric acid on thermo-mechanical properties of microcrystalline cellulose/polyvinyl alcohol blend and applicability as wood adhesive. *J. Adhes. Sci. Technol.* **2021**, *35*, 1072–1086. [[CrossRef](#)]
10. Alshahrani, A.A.; AlQahtani, M.; Almushaikeh, A.M.; Hassan, H.M.A.; Alzaid, M.; Alrashidi, A.N.; Alsouhaimi, I.H. Synthesis, characterization, and heavy-ion rejection rate efficiency of PVA/MWCNTs and Triton X-100/MWCNTs Buckypaper membranes. *J. Mater. Res. Technol.* **2022**, *18*, 2310–2319. [[CrossRef](#)]
11. Alrebdii, T.A.; Ahmed, H.A.; Alrefae, S.H.; Adel, R.; Toghan, A.; Mostafa, A.M.; Alkallas, F.H.; Rezk, R.A. Enhanced adsorption removal of phosphate from water by Ag-doped PVA-NiO nanocomposite prepared by pulsed laser ablation method. *J. Mater. Res. Technol.* **2022**, *20*, 4356–4364. [[CrossRef](#)]
12. Kalantari, K.; Mostafavi, E.; Saleh, B.; Soltantabar, P.; Webster, T.J. Chitosan/PVA hydrogels incorporated with green synthesized cerium oxide nanoparticles for wound healing applications. *Eur. Polym. J.* **2020**, *134*, 109853. [[CrossRef](#)]
13. Zhang, H.; Wu, K.; Jiao, E.; Chen, B.; Shi, J.; Lu, M. Greatly improved thermal conductivity and electrical insulation for PVA composites via introducing functional carbon nitride nanosheets. *Eur. Polym. J.* **2021**, *159*, 110718. [[CrossRef](#)]
14. Lei, Y.; Mao, L.; Yao, J.; Zhu, H. Improved mechanical, antibacterial and UV barrier properties of catechol-functionalized chitosan/polyvinyl alcohol biodegradable composites for active food packaging. *Carbohydr. Polym.* **2021**, *264*, 117997. [[CrossRef](#)] [[PubMed](#)]
15. Abrial, H.; Kadriadi; Mahardika, M.; Handayani, D.; Sugiarti, E.; Muslimin, A.N. Characterization of disintegrated bacterial cellulose nanofibers/PVA bionanocomposites prepared via ultrasonication. *Int. J. Biol. Macromol.* **2019**, *135*, 591–599. [[CrossRef](#)] [[PubMed](#)]
16. Yihun, F.A.; Ifuku, S.; Saimoto, H.; Yihun, D.A. Thermo-mechanically improved polyvinyl alcohol composite films using maleated chitin nanofibers as nano-reinforcement. *Cellulose* **2021**, *28*, 2965–2980. [[CrossRef](#)]
17. Menazea, A.A.; Ismail, A.M.; Awwad, N.S.; Ibrahim, H.A. Physical characterization and antibacterial activity of PVA/Chitosan matrix doped by selenium nanoparticles prepared via one-pot laser ablation route. *J. Mater. Res. Technol.* **2020**, *9*, 9598–9606. [[CrossRef](#)]
18. Abrial, H.; Ariksa, J.; Mahardika, M.; Handayani, D.; Aminah, I.; Sandrawati, N.; Sapuan, S.M.; Ilyas, R.A. Highly transparent and antimicrobial PVA based bionanocomposites reinforced by ginger nanofiber. *Polym. Test.* **2019**, *81*, 106186. [[CrossRef](#)]

19. Mahardika, M.; Abrial, H.; Kasim, A.; Arief, S.; Hafizulhaq, F.; Asrofi, M. Properties of cellulose nanofiber/bengkoang starch bionanocomposites: Effect of fiber loading. *LWT—Food Sci. Technol.* **2019**, *116*, 108554. [[CrossRef](#)]
20. Lim, M.; Kwon, H.; Kim, D.; Seo, J.; Han, H.; Khan, S.B. Highly-enhanced water resistant and oxygen barrier properties of cross-linked poly(vinyl alcohol) hybrid films for packaging applications. *Prog. Org. Coat.* **2015**, *85*, 68–75. [[CrossRef](#)]
21. Gadhave, R.V.; Dhawale, P.V.; Gadekar, P.T. Effect of boric acid on poly vinyl alcohol- tannin blend and its application as water-based wood adhesive. *Des. Monomers Polym.* **2020**, *23*, 188–196. [[CrossRef](#)] [[PubMed](#)]
22. Dhawale, P.V.; Vineeth, S.K.; Gadhave, R.V.; Fatima, M.J.; Supekar, M.V.; Thakur, V.K.; Raghavan, P. Tannin as a renewable raw material for adhesive applications: A review. *Mater. Adv.* **2022**, *3*, 3365–3388. [[CrossRef](#)]
23. Wang, Y.; Li, T.; Ma, P.; Bai, H.; Xie, Y.; Chen, M.; Dong, W. Simultaneous Enhancements of UV-Shielding Properties and Photostability of Poly(vinyl alcohol) via Incorporation of Sepia Eumelanin. *ACS Sustain. Chem. Eng.* **2016**, *4*, 2252–2258. [[CrossRef](#)]
24. Zhao, Z.; Mao, A.; Gao, W.; Bai, H. A facile in situ method to fabricate transparent, flexible polyvinyl alcohol/ZnO film for UV-shielding. *Compos. Commun.* **2018**, *10*, 157–162. [[CrossRef](#)]
25. Posoknistakul, P.; Tangkrakul, C.; Chaosuanphae, P.; Deepentharn, S.; Techasawong, W.; Phonphirunrot, N.; Bairak, S.; Sakdaronarong, C.; Laosiripojana, N. Fabrication and characterization of lignin particles and their ultraviolet protection ability in PVA composite film. *ACS Omega* **2020**, *5*, 20976–20982. [[CrossRef](#)]
26. Yang, W.; Ding, H.; Qi, G.; Li, C.; Xu, P.; Zheng, T.; Zhu, X.; Kenny, J.M.; Puglia, D.; Ma, P. Highly transparent PVA/nanolignin composite films with excellent UV shielding, antibacterial and antioxidant performance. *React. Funct. Polym.* **2021**, *162*, 104873. [[CrossRef](#)]
27. Zhai, Y.; Wang, J.; Wang, H.; Song, T.; Hu, W.; Li, S. Preparation and characterization of antioxidative and UV-protective larch bark tannin/PVA composite membranes. *Molecules* **2018**, *23*, 2073. [[CrossRef](#)]
28. Abrial, H.; Ikhsan, M.; Rahmadiawan, D.; Handayani, D.; Sandrawati, N.; Sugiarti, E.; Novi, A. Anti-UV, antibacterial, strong, and high thermal resistant polyvinyl alcohol/Uncaria gambir extract biocomposite film. *J. Mater. Res. Technol.* **2022**, *17*, 2193–2202. [[CrossRef](#)]
29. Abrial, H.; Kurniawan, A.; Rahmadiawan, D.; Handayani, D.; Sugiarti, E.; Muslimin, A.N. Highly antimicrobial and strong cellulose-based biocomposite film prepared with bacterial cellulose powders, Uncaria gambir, and ultrasonication treatment. *Int. J. Biol. Macromol.* **2022**, *208*, 88–96. [[CrossRef](#)]
30. Rahmadiawan, D.; Fuadi, Z.; Kurniawan, R.; Abrial, H.; Ilhamsyah, F. Tribology in Industry Tribological Properties of Aqueous Carboxymethyl Cellulose/Uncaria Gambir Extract as Novel Anti-Corrosion Water-Based Lubricant. *Tribol. Ind.* **2022**. [[CrossRef](#)]
31. ASTM D1003; Standard Test Method for Haze and Luminous Transmittance of Transparent Plastics. American Society for Testing and Materials: West Conshohocken, PA, USA, 2006.
32. ASTM D638-V; Standard Test Method for Tensile Properties of Thin Plastic Sheeting. American Society for Testing and Materials: West Conshohocken, PA, USA, 2012.
33. Ricciardi, R.; Auriemma, F.; De Rosa, C.; Lauprêtre, F. X-ray Diffraction Analysis of Poly(vinyl alcohol) Hydrogels, Obtained by Freezing and Thawing Techniques. *Macromolecules* **2004**, *37*, 1921–1927. [[CrossRef](#)]
34. Abrial, H.; Ariksha, J.; Mahardika, M.; Handayani, D.; Aminah, I.; Sandrawati, N.; Sugiarti, E.; Muslimin, A.N.; Rosanti, S.D. Effect of heat treatment on thermal resistance, transparency and antimicrobial activity of sonicated ginger cellulose film. *Carbohydr. Polym.* **2020**, *240*, 116287. [[CrossRef](#)] [[PubMed](#)]
35. Prodpran, T.; Benjakul, S.; Phatcharant, S. Effect of phenolic compounds on protein cross-linking and properties of film from fish myofibrillar protein. *Int. J. Biol. Macromol.* **2012**, *51*, 774–782. [[CrossRef](#)] [[PubMed](#)]
36. Sadeghifar, H.; Venditti, R.; Jur, J.; Gorga, R.E.; Pawlak, J.J. Cellulose-Lignin Biodegradable and Flexible UV Protection Film. *ACS Sustain. Chem. Eng.* **2017**, *5*, 625–631. [[CrossRef](#)]
37. Zayat, M.; Garcia-Parejo, P.; Levy, D. Preventing UV-light damage of light sensitive materials using a highly protective UV-absorbing coating. *Chem. Soc. Rev.* **2007**, *36*, 1270–1281. [[CrossRef](#)] [[PubMed](#)]
38. Abrial, H.; Fajrul, R.; Mahardika, M.; Handayani, D.; Sugiarti, E.; Muslimin, A.N.; Rosanti, S.D. Improving impact, tensile and thermal properties of thermoset unsaturated polyester via mixing with thermoset vinyl ester and methyl methacrylate. *Polym. Test.* **2020**, *81*, 106193. [[CrossRef](#)]
39. Chen, J.; Li, Y.; Zhang, Y.; Zhu, Y. Preparation and characterization of graphene oxide reinforced PVA film with boric acid as crosslinker. *J. Appl. Polym. Sci.* **2015**, *132*, 42000. [[CrossRef](#)]
40. Hong, X.; He, J.; Zou, L.; Wang, Y.; Li, Y.V. Preparation and characterization of high strength and high modulus PVA fiber via dry-wet spinning with cross-linking of boric acid. *Appl. Polym. Sci.* **2021**, *138*, 51394. [[CrossRef](#)]
41. Miyazaki, T.; Takeda, Y.; Akane, S.; Itou, T.; Hoshiko, A.; En, K. Role of boric acid for a poly (vinyl alcohol) film as a cross-linking agent: Melting behaviors of the films with boric acid. *Polymer* **2010**, *51*, 5539–5549. [[CrossRef](#)]
42. Ilyas, R.A.; Sapuan, S.M.; Ishak, M.R.; Zainudin, E.S. Sugar palm nanofibrillated cellulose (*Arenga pinnata* (Wurmb.) Merr): Effect of cycles on their yield, physic-chemical, morphological and thermal behavior. *Int. J. Biol. Macromol.* **2019**, *123*, 379–388. [[CrossRef](#)]
43. Asrofi, M.; Abrial, H.; Kasim, A.; Pratoto, A.; Mahardika, M.; Hafizulhaq, F. Characterization of the Sonicated Yam Bean Starch Bionanocomposites Reinforced By Nanocellulose Water Hyacinth Fiber (Whf): The Effect of Various Fiber Loading. *J. Eng. Sci. Technol.* **2018**, *13*, 2700–2715.

44. Kaewprachu, P.; Rungraeng, N.; Osako, K.; Rawdkuen, S. Properties of fish myofibrillar protein film incorporated with catechin-Kradon extract. *Food Packag. Shelf Life* **2017**, *13*, 56–65. [[CrossRef](#)]
45. Hong, K.H. Preparation and properties of polyvinyl alcohol/tannic acid composite film for topical treatment application. *Fibers Polym.* **2016**, *17*, 1963–1968. [[CrossRef](#)]
46. De Menezes, B.R.C.; Ferreira, F.V.; Silva, B.C.; Simonetti, E.A.N.; Bastos, T.M.; Cividanes, L.S.; Thim, G.P. Effects of octadecylamine functionalization of carbon nanotubes on dispersion, polarity, and mechanical properties of CNT/HDPE nanocomposites. *J. Mater. Sci.* **2018**, *53*, 14311–14327. [[CrossRef](#)]
47. Nandika, D.; Syamsu, K.; Arinana; Kusumawardhani, D.T.; Fitriana, Y. Bioactivities of catechin from gambir (*uncaria gambir roxb.*) against wood-decaying fungi. *BioResources* **2019**, *14*, 5646–5656. [[CrossRef](#)]
48. Gutiérrez-del-Río, I.; Fernández, J.; Lombó, F. Plant nutraceuticals as antimicrobial agents in food preservation: Terpenoids, polyphenols and thiols. *Int. J. Antimicrob. Agents* **2018**, *52*, 309–315. [[CrossRef](#)]
49. Xu, Z.; Du, P.; Meiser, P.; Claus, J. Proanthocyanidins: Oligomeric structures with unique biochemical properties and great therapeutic promise. *Nat. Prod. Commun.* **2012**, *7*, 381–388. [[CrossRef](#)]